A Mobile Vision-based System for Gap and Flush Measuring between Planar Surfaces using ArUco Markers

Long Hoang Pham[1], Duong Nguyen-Ngoc Tran[1], Chul Hong Rhie[2], and Jae Wook Jeon[1]
[1] *Sungkyunkwan University, Department of Electrical and Computer Engineering*
[2] *Advanced Manufacturing CAE Team, Hyundai Motor Company*
South Korea
phlong@skku.edu, duongtran@skku.edu, 2fered@hyundai.com, jwjeon@yurim.skku.ar.kr

2021 International Conference on Electronics, Information, and Communication (ICEIC) | 978-1-7281-9161-4/21/$31.00 ©2021 IEEE | DOI: 10.1109/ICEIC51217.2021.9369720

***Abstract*—The dimensional inspection of the gap and flush (GF) created by two different surfaces has been a long-standing and challenging field of research. In this paper, a novel mobile vision-based measurement system has been developed with the goal to detect and measure the gap accurately. ArUco markers have been attached to two planar surfaces. A sequence of images is captured, and the 3D information of markers are estimated. The flush is the difference between the depth information obtained from the markers, while the width can be converted from the image using the pixel resolution computed from the marker's physical size. A working prototype of the proposed method has been implemented and extensively evaluated on synthetic gaps. The experimental results validate the robustness and applicability of the proposed method in a real-world environment.**

Keywords— ArUco marker; image processing; gap flush measurement

I. INTRODUCTION

The measurement of the gap and flush (GF) between two planar surfaces has been a well-established and constant problem in many sectors of research and industry, for instance in automobile manufacturing or construction [1, 2]. However, the GF measuring process is still performed using mechanical devices: feeler gauge or taper welding gauge, which is not only subjected to high human errors but is also tedious and time-consuming which results in high labor costs. While in some areas, microscopic inspection of the gap is performed using special tools like laser-based, ultrasound-based, or electrical-based sensors. These tools are expensive and required regular maintenance which adds up tremendously to overall operation cost.

Smartphones have been utilized as versatile digital instruments for various applications [3-6] because they have cameras, an operation unit, and various inertial sensors in a self-contained package that is cheap, easily affordable, and accessible by most researchers and practitioners.

In this paper, a mobile vision-based gap-measuring system has been developed using only images acquired by a smartphone camera. The proposed method combines techniques of computer vision and fiducial markers to detect GF automatically in images and techniques of pose estimation and statistical estimation to measure the GF. The main contribution and novelty of the proposed approach lie in the use of smartphones and ArUco markers to identify and measure GF in real-time. Moreover, the use of ArUco markers [7-9] placed on the measured gap as the features for both identification and measuring intro- duces an improvement over the drawback of non-robust and computationally intensive processing of previous vision-based methods. Also, the proposed method relies on the idea that the camera 3D pose, given it is calibrated, can be estimated from markers four-corners [7], hence providing monocular cameras with the deep-sensing capability and thus allowing the possibility of flush measuring by differentiating the depth readings between a pair of markers. Several experiments were conducted in a controlled environment and the results are compared with the manual inspection method.

The paper begins by describing the related works in Section 2 discusses the proposed method which includes the GF detection algorithm and the GF measurement algorithm. Section 3 gives an exhaustive analysis of the experimental results. Finally, Section 4 presents the conclusion.

II. THE PROPOSED METHOD

A. Gap and Flush Detection

The image processing comprises several steps aimed at detecting the gap edges and extracting the gap points from them. While the image analysis is not a novel contribution, the gap

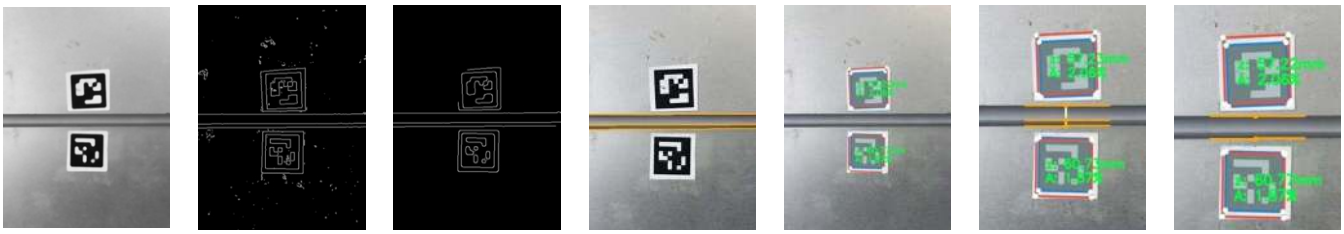

(a) (b) (c) (d) (e) (f) (g)

Fig. 1: GF detection algorithm. a) Input image. b) Edge detection results on the input image. c) Edge detection results on the median filtered image. d) Gap line extraction. e) ArUco markers detection. f) Detecting all possible gap points. g) Final results of GF detection.

points detection is a new approach specifically designed to use in combination with the ArUco markers.

First, the captured image is converted from an RGB image into a grayscale image. Then median filtering with a kernel window of 5×5 is applied over the image. The pixels in the kernel window are ranked according to the pixel value and then selecting the middle value of the group as the output pixel. From Fig. 1b and c, the median filtering can remove strong and isolated noises while maintaining the sharpness of the most prominent contours in the image.

Second, the edges are extracted using Canny edge detector. The low and high thresholds of the image are determined by:

$$\begin{aligned} lt &= \max(0, (1.0 - \sigma_1) \times \tilde{m}) \\ ht &= \min(0, (1.0 + \sigma_1) \times \tilde{m}) \end{aligned} \quad (1)$$

where $\sigma_1 = 0.3$, and $\tilde{m}$ is the median value of the image. The edge image can be found in Fig. 1c. The contour extraction is performed on the edge image using the Suzuki and Abe's border following algorithm [10]. It produces a set of image contours as shown in Fig. 1c. Then, a polygonal approximation is performed using the Douglas-Peucker algorithm [11]. Since gap edges are mostly straight lines, when enclosed in a rectangular contour, these are approximate to long and narrow four-vertex polygons. Meanwhile, markers contours can be approximately square polygons. A ratio function $R(c_i)$ is introduced to classify each contour into either marker contours or gap line contours as follow:

$$\begin{cases} c_i = M & \text{if } R(c_i) \le \sigma_2 \\ c_i = L & \text{if } R(c_i) > \sigma_2 \end{cases}$$
$$\text{with,} \quad R(c_i) = \frac{\min[B_l(c_i), B_w(c_i)]}{\max[B_l(c_i), B_w(c_i)]} \quad (2)$$

where M and L denotes the set of marker contours and gap lines respectively. $B_l(c_i)$ and $B_w(c_i)$ are the length and width of the bounding box of each contour c_i respectively. Using $\sigma_2 = 0.1$ the gap edges can be obtained as shown in Fig. 1d.

Fourth, ArUco marker detection, which is a well-defined process in the literature [7-9], is applied to identify the markers from the extracted candidates in prior step and obtain their locations in the image. Each identified marker is further simplified as an array of 5 points $m_i = \{p_j \,|j = 0, .., 4\}$ where p_0 is the center point and the rests are the four corners. The detected ArUco markers are illustrated in Fig. 1e.

Finally, gap points extraction is extracted from the set of line contours L. For that purpose, a line is projected by connecting markers centers. Let denote this line as l_0: $a_0x + b_0y = c_0$. The interception between l_0 and each gap line l_i: $a_ix + b_iy = c_i \in L$ will result in a gap point $g_i(x, y)$ with:

$$g_i(x) = \frac{c_0b_i - c_ib_0}{a_0b_i - a_ib_0}; \quad g_i(y) = \frac{c_ia_0 - c_0a_i}{a_0b_i - a_ib_0} \quad (3)$$

Ideally, two gap points are extracted for a gap; however, in some cases, the gap points of the internal edges are also detected in the image as shown in Fig. 1f. In these cases, only the outermost gap points are considered valid and the inner gap points are discarded. The final results in this step is illustrated in Fig. 3g.

B. Gap and Flush Measurement

The proposed GF measurement method consists of two steps: calculating width value using pixel resolution and estimating flush value using pose estimation. The gap is estimated from the pixel resolution multiplied by the number of pixels between the gap points detected by the GF detection algorithm.

$$G = \frac{|ax + by + c|}{\sqrt{a^2 + b^2}} \times \rho \quad (4)$$

where g is the gap measurement, x and y are the coordinates of the gap point, ρ is the pixel resolution. The pixel resolution can be obtained through markers, by calculating the ratio between the known physical dimension and the detected pixel dimensions.

Meanwhile, the flush is computed from the difference in depth between the two surfaces. In the case of a monocular camera, depth sensing capability is possible by utilizing the pose estimation algorithm. Let us first define two coordinate systems: the camera (Σ_{CAM}) and the image coordinate (Σ_{IP}) systems. Since smartphone cameras also follow the pinhole camera mode, the imaging process is typically modeled by a perspective transform. In this model, a point $P = [X, Y, Z, 1]^T$ in the 3D camera

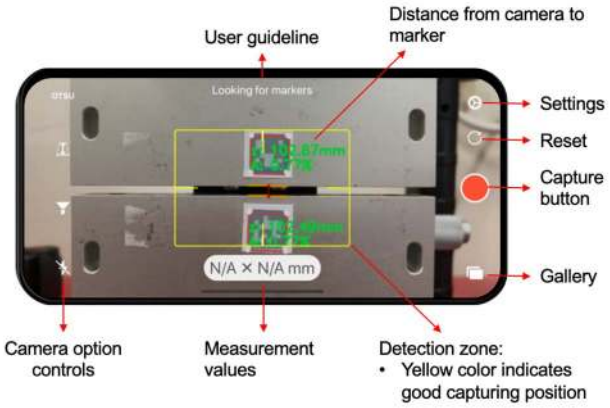

Fig. 3: The user interface of the GF detection and measurement algorithm

coordinate system is mapped to a point $p = [x, y, 1]^T$ in the 2D image plane following the matrix-vector product formula:

$$\begin{bmatrix} x \\ y \\ 1 \end{bmatrix} = \begin{bmatrix} \alpha_x & 0 & c_x \\ 0 & \alpha_y & c_y \\ 0 & 0 & 1 \end{bmatrix} \begin{bmatrix} r_{00} & r_{10} & r_{20} & t_x \\ r_{01} & r_{11} & r_{21} & t_y \\ r_{02} & r_{12} & r_{22} & t_z \end{bmatrix} \begin{bmatrix} X \\ Y \\ Z \\ 1 \end{bmatrix} \quad (5)$$

where $\alpha_x, \alpha_y, c_x, c_y$ are the intrinsic parameters obtained from the camera calibration process as shown in Fig. 2c. α_x, α_y are the focal length in x- and y-axis (in pixels) and c_x, c_y are the coordinates of the principal point (i.e., the center) of the image plane.

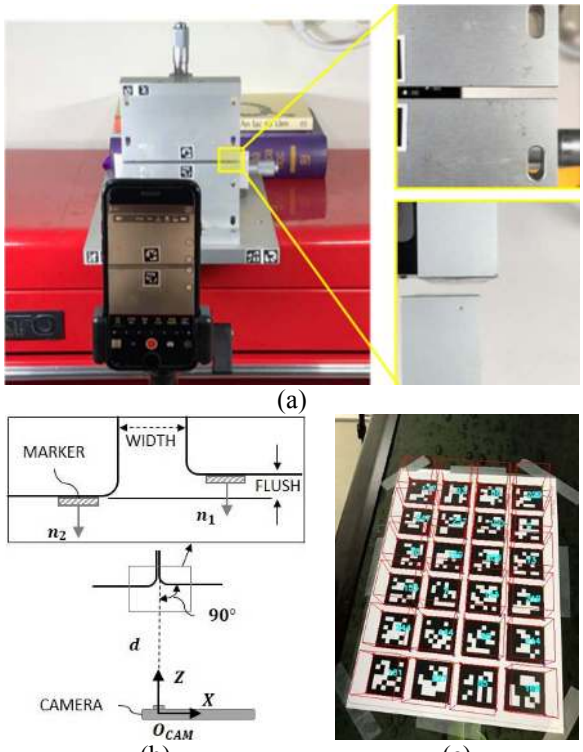

Fig. 2: a) The experimental setup. b) Definition of gap and flush between two planar surfaces. c) The calibration board using series of ArUco markers.

From Equation (5), estimating the pose of a 3D object means finding six numbers, three for translation and three for rotation. Equation (5) can be solved using the Infinitesimal Plane-based Pose Estimation (IPPE) method [12]. IPPE method is a straightforward, computationally efficient solution to compute a planar object 3D pose from a single image from four points correspondences. Now, to estimate the flush value, we extracted translations in z-axis (t_z) of both markers poses and calculated the absolute difference between them:

$$F = |T_0(t_z) - T_1(t_z)| \quad (6)$$

where T_0 and T_1 are the translation vector of two detected markers respectively.

III. Experiment and Discussion

A. Experimental Setup

The experimental setup consists of a smartphone (Apple iPhone 7) implementing the GF detection and measurement algorithms. A user interface, as shown in Fig. 3, was implemented to help the user perform the measurement easily. ArUco markers are printed on sticky label paper and attached on the testing specimen as shown in Fig. 2a. The testing specimen's gap and flush can be adjusted. The ground-truth values of GF were measured using a digital flush gauge and a digital vernier caliper with an uncertainty of ±0.01 mm. The experiments were performed indoors with constant lighting conditions.

In order to measure the GF, it is necessary to know the camera pixel resolution and intrinsic parameter. A camera calibration routine [13] using a chessboard of ArUco markers was performed. From a sequence of images of the chessboard in different positions and orientation, the toolbox returns the estimated parameter. The toolbox outputs many parameters, such as the intrinsic matrix of calibration, lens distortion, and others. However, for this paper, the only needed parameter is the intrinsic matrix. However, note that this value is used without any loss of generality and if a new camera was to be used, a new calibration procedure must be performed.

B. Results and Discussion

To assess the accuracy of the GF measurement algorithm proposed in this paper an evaluation had to be performed. Therefore, several specimens with known dimensions were scanned with the apparatus to obtain a quantitative assessment of the accuracy. The resulting measurements were then compared to the actual dimensions. The results of this comparison is shown in Table 1. The first column is the number of the measure object. The next six columns show the actual gap value, the mean of the measured gap, the standard deviation, the standard uncertainty, the absolute error between the mean and actual gap, and finally the relative error, respectively. The next six columns are the

TABLE 1: Results from GF Measurement of the Specimen.

	GAP						FLUSH					
#	GT (mm)	Mean (mm)	Std. Dev. (mm)	Std. Unc. (mm)	Offset (mm)	Rel. Err. (%)	GT (mm)	Mean (mm)	Std. Dev. (mm)	Std. Unc. (mm)	Offset (mm)	Rel. Err. (%)
1	2.500	2.539	0.003	0.001	0.039	1.56	2.500	2.431	0.025	0.008	0.069	2.76
2	2.600	2.652	0.030	0.010	0.052	2.00	2.600	2.652	0.088	0.028	0.052	2.00
3	2.700	2.748	0.004	0.001	0.048	1.78	2.700	2.731	0.084	0.027	0.031	1.15
4	2.800	2.860	0.000	0.000	0.060	2.14	2.800	2.749	0.054	0.017	0.051	1.82
5	2.900	2.840	0.004	0.001	0.060	2.07	2.900	2.937	0.072	0.023	0.037	1.28
6	3.000	2.949	0.003	0.001	0.051	1.70	3.000	3.087	0.042	0.013	0.087	2.90
7	3.100	3.080	0.000	0.000	0.020	0.65	3.100	3.047	0.040	0.013	0.053	1.71
8	3.200	3.162	0.004	0.001	0.038	1.19	3.200	3.226	0.043	0.014	0.026	0.81
9	3.300	3.299	0.003	0.001	0.001	0.03	3.300	3.394	0.041	0.013	0.094	2.85
10	3.400	3.361	0.035	0.011	0.039	1.15	3.400	3.464	0.056	0.018	0.064	1.88
11	3.500	3.542	0.026	0.008	0.042	1.20	3.500	3.435	0.024	0.008	0.065	1.86
	Worst-case		0.035	0.011	Avg.	1.41	Worst-case		0.088	0.028	Avg.	1.91

similar for the flush measurement. The evaluation results presented in Table 1 imply that the accuracy of the GF detection and measurement is high enough to distinguish between typical GF between two planar surfaces which are assumed to have a minimal difference of 0.5 mm. The uncertainty of the measurement process is determined by the worst-case value: 0.011 mm for gap and 0.028 mm for flush. A statistical analysis demonstrates that the average error is small, demonstrating the accuracy of the measurement.

IV. Conclusion

This paper presented a new methodology to detect and measure GF using smartphone and ArUco markers. The proposed method allows for allows for quick and accurate measurement in workplaces that requires constant inspection of gaps between two planar surfaces. According to the method, a sequence of images is captured using the smartphone. The algorithm receives images as inputs and outputs a new image that highlights the ArUco markers and gap points. Then the markers poses are estimated using camera intrinsic parameters and the flush value is calculated from finding the difference between the poses of two markers. The gap is estimated by counting the number of pixels between the gap points multiplied with the pixel resolution obtained using the marker dimensions. The statistical analysis demonstrates that the error is small on average permitting the accurate measurement.

References

[1] D. Kosmopoulos and T. Varvarigou, "Automated Inspection of Gaps on the Automobile Production Line Through Stereo Vision and Specular Reflection," Computer in Industry, vol. 46, no. 1, pp. 49–63, 2001.

[2] S. Lee and C. Jun, "Identifying Sources of Dimensional Variation Affecting Assembly Quality of Automobiles," in Proceedings of the 9th APIEMS Conference, 2008.

[3] B.-Y. Chang, "Smartphone-based Chemistry Instrumentation: Digitization of Colorimetric Measurements," Bulletin of the Korean Chemical Society, vol. 33, no. 2, pp. 549–552, 2012.

[4] S. Choi, S. Kim, J.-S. Yang, J.-H. Lee, C. Joo, and H.-I. Jung, "Real-time Measurement of Human Salivary Cortisol for the Assessment of Psychological Stress Using a Smartphone," Sensing and Bio-Sensing Research, vol. 2, pp. 8 – 11, 2014.

[5] A. Hossain, J. Canning, S. Ast, P. J. Rutledge, T. L. Yen, and A. Jamalipour, "Lab-in-a-phone: Smartphone-based Portable Fluorometer for pH Measurements of Environmental Water," IEEE Sensor Journal, vol. 15, no. 9, pp. 5095–5102, 2015.

[6] J. H. Gao and L. S. Peh, "A Smartphone-based Laser Distance Sensor for Outdoor Environments," Proceeding of the IEEE International Conference on Robotics and Automation, pp. 2922–2929, 2016.

[7] S. Garrido-Jurado, R. Munoz-Salinas, F. J. Madrid-Cuevas, and M. J. Marın-Jimenez, "Automatic Generation and Detection of Highly Reliable Fiducial Markers Under Occlusion," Pattern Recognition, vol. 47, no. 6, pp. 2280–2292, 2014.

[8] S. Garrido-Jurado, R. Munoz-Salinas, F. J. Madrid-Cuevas, and M. J. Marın-Jimenez, "Generation of Fiducial Marker Dictionaries using Mixed Integer Linear Programming," Pattern Recognition, vol. 51, pp. 481–491, 2016.

[9] F. J. Romero-Ramirez, R. Munoz-Salinas, and R. Medina-Carnicer, "Speeded Up Detection of Squared Fiducial Markers," Image and Vision Computing, vol. 76, pp. 38–47, 2018.

[10] S. Suzuki and K. Abe, "Topological Structural Analysis of Digitized Binary Images by Border Following," Computer Vision, Graphics, and Image Processing, vol. 46, pp. 32–46, 1985.

[11] D. H. Douglas and T. K. Peucker, "Algorithms for the Reduction of the Number of Points Required to Represent a Digitized Line or Its Caricature," Cartographical: The International Journal for Geographic Information and Geovisualization, no. 10, pp. 112–122, 1973.

[12] T. Collins and A. Bartoli, "Infinitesimal Plane-based Pose Estimation," International Journal of Computer Vision, vol. 109, no. 3, pp. 252–286, 2014.

[13] W. Burger, "Zhang's Camera Calibration Algorithm: In-Depth Tutorial and Implementation," p. 56.